Impact of laser stacking and photocathode materials on microbunching stability in photoinjectors

S. Bettoni,* M. Csatari Divall, R. Ganter, M. Pedrozzi, E. Prat, S. Reiche, T. Schietinger, A. Trisorio, and C. Vicario
Paul Scherrer Institut, 5232 Villigen, Switzerland

V. Goryashko
Department of Physics and Astronomy, Uppsala University, 75120 Uppsala, Sweden

(Received 7 October 2019; accepted 29 January 2020; published 12 February 2020)

Microbunching instability is a well-known phenomenon that may deteriorate the performance of accelerators. The instability may be triggered by a shot-noise mechanism or by some initial intensity modulations at the generation of the electron bunch (or both) and can be amplified all along the machine. At SwissFEL, the free-electron laser (FEL) facility operating at the Paul Scherrer Institute (PSI), the initial design stipulated a shaping of the photocathode laser output to obtain a flat-top longitudinal profile. This scheme is attractive in terms of the uniformity of the beam properties along the bunch. The drawback of this approach is that some unavoidable modulations are generated along the laser pulse. We investigate, both experimentally and by numerical simulations, the longitudinal dynamics of a beam obtained illuminating a copper cathode with a laser profile shaped by the stacking technique. We repeat the analysis for several compression factors and initial laser profile modulations. We find that the microbunching instability gain renders the use of the stacking technique not efficient to run a free-electron laser facility using as photocathode a material with a short response time. We experimentally demonstrate that the use of a material with a longer response time efficiently damps the structures originating from the laser profile obtained with stacking, and helps to improve the performance of the facility. In general, this is an approach to minimize the microbunching instability at any FEL (also not using stacking) or at least reduce the use of other countermeasures, which, such as the laser heater, may degrade the final FEL performance.

DOI: 10.1103/PhysRevAccelBeams.23.024401

I. INTRODUCTION

In the last years several free-electron laser (FEL) facilities have been built or are under construction with the aim of generating high-power coherent x-ray radiation, which is used for applications in physics, biology and material science. The majority of the FELs use photoinjectors [1] to generate the suitable electron beams. At the source, relatively long bunches (from 1 to 10 ps) are typically produced to counteract effects from space-charge forces at low energy. Downstream of the first acceleration stage (typically at beam energies of a few hundreds of MeV) the bunch is compressed in one or more stages to produce very high current beams (typically a few kA of peak current), necessary to reach a significant lasing intensity.

Numerous FEL measurements showed self-developing modulations in the longitudinal phase space of compressed electron bunches [2,3]. The mechanism of this phenomenon is known as microbunching instability. Modulations along the current profile of the beam develop into energy structures. This is because the electrons in the bunch repel each other and initiate space-charge oscillations, which transfer the initial modulation of the current profile to the energy distribution. At the first bunch compressor the energy modulation is converted to density oscillations, due to the dependence of the path length of the beam trajectory on the particles' energies in dispersive sections. Any downstream compression stages further amplify such current and energy modulations. The final result can be that the beam longitudinal phase space is so heavily distorted that it prevents the beam from lasing or generates an undesirable broadening of the radiation spectrum through the occurrence of side bands. Another harmful phenomenon associated to microbunching instability is the emission of intense coherent radiation. This radiation may be so intense that optical transition radiation (OTR) screens,

*simona.bettoni@psi.ch

Published by the American Physical Society under the terms of the Creative Commons Attribution 4.0 International license. Further distribution of this work must maintain attribution to the author(s) and the published article's title, journal citation, and DOI.

typically used to perform beam profile measurements, become saturated and hence unusable. However, this limitation can be overcome by using wire scanners or a recently developed new type of monitors [4].

The microbunching instability is mainly determined by the modulations generated at the source and shot noise, and their amplification at the compression stages. Here we focus on the first source. The amplification is quantified by the microbunching instability gain curve, the ratio of the amplitude of a current modulation at any location over that at the beginning of the machine or in general upstream of the first compression stage as a function of the initial modulation frequency. This gain curve is determined by the beam and machine parameters, such as the gradients and lengths of the accelerating cavities, and the compression setup.

A possible way to reduce the gain is to induce, in a controlled way, disorder in the electron bunch. Among several options that have been proposed, based on, e.g., phase mixing [5], transverse gradient undulators [3], optical klystron [6], or rf deflecting cavities [7], the so-called laser heater [8,9] is the most commonly applied method. This device was demonstrated to be a very efficient tool to strongly reduce the amplification process. The laser heater (LH) system consists of a magnetic chicane, where an undulator module is installed to allow resonant energy exchange between the electron bunch and a copropagating laser. The laser heater damps the instability by increasing the uncorrelated energy spread of the bunch, thereby reducing the amplification gain via Landau damping in the downstream sections of the machine. The Linac Coherent Light Source (LCLS) was the first facility to demonstrate that an improvement of the FEL performance is achievable by use of a laser heater [8]. A drawback of this method consists in the degradation of the beam longitudinal emittance, and therefore the lasing performance, as a consequence of the associated increase of the electron bunch energy spread.

An important beam property in view of FEL lasing intensity is the uniformity, along the bunch, of vital beam parameters such as emittance and optics matching. The more uniform these parameters are along the bunch, the more balanced is the lasing for the full length of the beam. The settings that are optimal for lasing are then the same for a majority of the bunch slices, and consequently, the FEL signal can readily be maximized. One way to achieve such uniform parameters is to use a flat-top as the longitudinal profile of the laser illuminating the photocathode. Such a profile can be approximated by stacking several pulses in time. This procedure, however, inevitably leads to some intensity modulations on the laser profile. In this paper we study the dynamics of electron bunches generated by illuminating a photocathode with a laser pulse whose profile is shaped via the stacking technique for a copper cathode. We find, both in measurements and in simulations, that the amplitude of the unavoidable modulations of the laser profile impinged on the electron bunch strongly deform the beam longitudinal phase space even at relatively low compression factors. In the most extreme case we observe a splitting of each one of the stacked single pulses, driving the instability into a regime where the frequency of the final density modulations is different from the one at the beginning. This shifts the frequency content of the bunch longitudinal profile toward a region where the amplification gain of the microbunching is larger than what corresponds to the laser modulations. These effects lead us to conclude that the stacking technique is not well suited to drive an FEL photoinjector in case a fast response time material photocathodes (response time up to the few tens of fs) are used.

The above discussion is valid only if the photocathode is made of material characterized by a response time short compared to the periodicity of the modulations of the laser longitudinal profile. This is the case for a typical laser profile obtained with stacking and a copper cathode, where the response time is in the order of few tens of fs. For cathode materials characterized by a longer response time, like cesium telluride (Cs_2Te, response time in the range of a few hundreds of fs to 1 ps [10,11]), which we consider in this work, the structures impinged on the electron bunch by the laser profile are strongly smoothed out. In this situation the photocathode acts as a low-pass filter of the laser profile, damping the modulations in the frequency region where the gain curve has a maximum. In this case therefore the degradation of the quality of the electron beam is alleviated. This then opens up the possibility to still make use of the stacking technique for the generation of the laser profile without suffering its detrimental effect in terms of microbunching. As the source of the microbunching instability is strongly suppressed, it may be removed completely or the amount of energy spread required to be induced by the laser heater may be reduced significantly, such that the electron beam quality and consequently the FEL performance are not compromised.

In Sec. II we describe the SwissFEL facility and the SwissFEL Injector Test Facility (SITF) at the Paul Scherrer Institute. The measurements we present were performed at the SITF, in preparation for SwissFEL. We then present numerical simulations performed to determine the impact of the microbunching, the effect of the laser heater on the damping of the instability and on the FEL intensity at SwissFEL (Sec. III). We have also simulated the conditions which generate the splitting of the beam longitudinal phase space. In Sec. IV we present the measurements performed at the SITF to verify the key findings of the numerical simulations. In particular we have studied the evolution of the longitudinal phase space of a beam under compression in terms of amplification of the initial modulations, and we show the splitting of the beam longitudinal phase space. In Sec. IV B, finally, we demonstrate the efficient damping of

the laser modulations for a compressed bunch, comparing the beam longitudinal phase spaces obtained with copper and Cs_2Te photocathodes.

II. SWISSFEL AND THE SWISSFEL INJECTOR TEST FACILITY (SITF)

The simulations presented in this work were performed to estimate the microbunching gain as well as the impact of a laser heater on the resulting lasing performance at SwissFEL, the FEL facility at the Paul Scherrer Institute [12,13]. The SwissFEL commissioning of the hard X-ray line, Aramis, began in August 2016, with first pilot experiments at the end of 2017 and leading to the start of regular user operation in early 2019. The commissioning of the Athos line started in 2018 with first light expected by the end of 2019.

A schematic layout of the SwissFEL facility is shown in Fig. 1. In the photoinjector electrons are emitted from a cathode illuminated by a UV laser and then accelerated up to an energy of 7.1 MeV by an S-band rf gun. Downstream of the gun two S-band structures (2.998 GHz) operate at on-crest accelerating phase to boost the beam to an energy of 140 MeV. At this location the laser heater is installed [14]. Two more S-band cavities operate at off-crest accelerating phase to further increase the beam energy while simultaneously imposing the energy variation along the bunch necessary for the longitudinal compression at the first four-bend magnetic chicane (BC1). The bunch is compressed by a factor 10, to achieve a peak current of 200 A (starting from 20 A at the exit of the injector). Upstream of BC1 an X-band cavity (11.992 GHz, fourth harmonic of the main S-band frequency), linearizes the longitudinal phase space to ensure a uniform bunch compression. This first compression occurs at a beam energy of 300 MeV. The first C-band (5.712 GHz) linac (linac 1) boosts the beam energy up to 2.1 GeV. At this energy a second magnetic chicane (BC2) compresses the beam by a further factor of 15 to reach the 3 kA design peak current. Further downstream the beam is accelerated to 3.0 GeV (linac 2) and then either brought to the design energy of 5.8 GeV (linac 3) and sent to the Aramis hard-x-ray FEL line, or deflected into a dogleg and, after a possible energy adjustment, down the soft-x-ray FEL line Athos. SwissFEL operates at different charges ranging from 10 pC to 200 pC to fulfill the different user requests in terms of pulse duration and FEL intensity.

TABLE I. SwissFEL design parameters at the two compression stages BC1 and BC2 for the operation mode with maximum bunch charge.

	BC1	BC2
Beam energy (GeV)	0.30	2.10
Compression factor	10	18
Distance from cathode (m)	100	220
R_{56} (mm)	−55.0	−20.7

In this work we concentrate on the maximum charge mode, for which we list the most important compression parameters in Table I.

The measurements shown here were performed at the SITF, which operated between August 2010 and October 2014 to verify the design parameters and to test some of the most critical components of SwissFEL. The design of the SITF is similar to the first sections of SwissFEL down to the first bunch compressor, but without a laser heater and with a lower final energy of 250 MeV. The design compression factor is 10, but shorter bunches were obtained during the measurements discussed here. More detailed information on the facility and its commissioning can be found in [15].

The SITF gun laser featured a pulse stacking system [16,17] to produce flat-top like longitudinal laser profiles for the illumination of the cathode. The purpose of this system is to generate as uniform as possible mismatch and emittance along the bunch in view of maximizing the FEL intensity. The laser system is a Ti:Sapphire amplifier based on broadband chirped-pulse amplification [18]. The near infrared laser ($\lambda = 801$ nm) is frequency tripled into the ultra-violet ($\lambda = 267$ nm) spectral range using collinear harmonic generation in BBO crystals. The 50 fs short UV pulses are then stretched (employing a 10 cm long CaF_2 block) and subsequently sent into the temporal shaping stage.

Among various techniques used to obtain temporally flat-top-like picosecond UV pulses, pulse stacking with alpha-BBO crystals turned out to be the most efficient and robust with respect to the suitability for operation in large-scale research facilities. A schematic view of the stacking procedure is shown in Fig. 2. A number N of birefringent crystals of decreasing thickness are used to produce 2^N replicas of a single Gaussian pulse equally spaced in time.

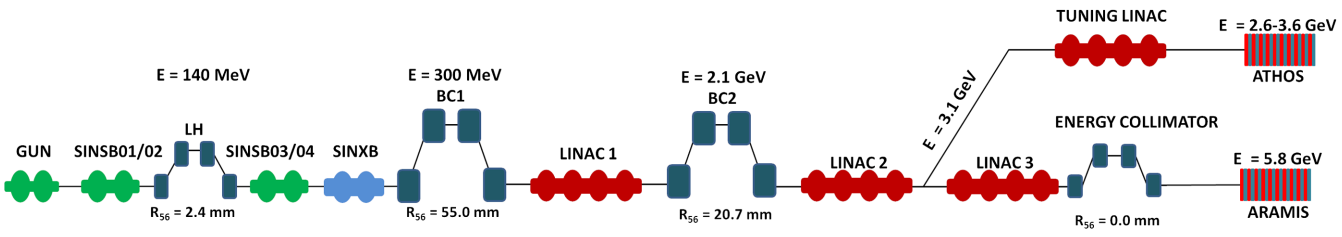

FIG. 1. SwissFEL schematic layout. The key parameters of the machine relevant for the discussion are also reported.

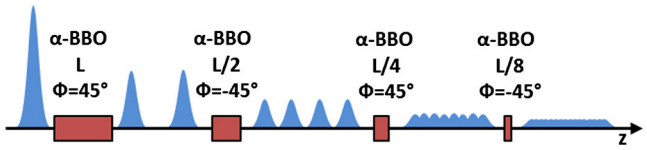

FIG. 2. Schematic view of the stacking process. The lengths and the relative orientations of the birefringent crystals are indicated. The shape of the final profile is changed by varying the orientation Φ of the single crystals.

A limitation of the stacking technique arises from the unavoidable amplitude modulations on the final profile. The length of the single stack is in fact limited by the possible interference pattern generated by the overlap of subsequent replicas of the same polarization state. Therefore some modulations must be expected due to the fact that a discrete finite number of subpulses with limited length add up to the final profile.

For the measurements discussed in Sec. IV we use the stacking scheme to generate longitudinal laser pulse profiles of 10 ps duration (full width at half maximum, FWHM), which corresponds to the design laser pulse for the SwissFEL 200 pC bunch charge mode. We deliberately change the number of replicas to study the effect of laser profile modulation depth and wavelength. Table II shows the frequencies corresponding to some of the possible settings of the stacking, obtained by changing the number of crystals while keeping the full length of the profile constant at 10 ps (FWHM).

In Table III we list the most relevant laser, electron bunch and machine parameters for the measurements reported in Sec. IV. We set the total pulse length and the transverse size of the laser to the design values corresponding to 200 pC bunch charge, but, in the case of the copper photocathode, the poor quantum efficiency of the cathode limited our measurements to a bunch charge of 100 pC. In this case our measurements therefore understate the effects from space charge with respect to the SwissFEL design.

TABLE II. Number of subpulses used to obtain the laser profile and corresponding wavelength of the modulation of the laser profile for a total pulse length of 10 ps (FWHM).

Number of subpulses	λ (μm)
8	375
16	188
32	94
64	47

TABLE III. Beam, photocathode, and machine parameters for the measurements described in Sec. IV.

Parameter	Value
Bunch charge (pC)	100 (Cu) or 200 (Cs_2Te)
Laser pulse length FWHM (ps)	9.9
Laser transverse beam size rms (mm)	0.2
Final bunch energy (MeV)	250
Compression factor	1–12

A cathode load-lock system [19], installed in the test facility in 2013, significantly facilitates the exchange of photocathodes in the gun since that time. Thanks to the system, the comparison between different photocathode materials has become relatively fast and reliable, as the time between measurements with different cathodes is minimized.

The photocathode materials compared in this work are copper and Cs_2Te. The copper cathode we use is a standard oxygen-free-copper monocrystal, whereas the Cs_2Te cathode was produced in-house according to a procedure developed by CERN [20]. The latter is a copper plug coated with about 15 nm of telluride and 25 nm of cesium sequentially evaporated. The deposition is done in the laboratory and the coated plugs are then transported to the gun under vacuum in a vacuum suitcase. They are then transferred to the backplane of the rf gun using the load-lock system.

III. NUMERICAL SIMULATIONS

As a first part of our discussion we investigate the enhancement of any pre-existing bunching in the electron beam line along SwissFEL toward the Aramis hard-x-ray FEL line, following an approach similar to the one described in Refs. [21,22]. The function describing this enhancement is solely determined by the machine layout and the bunch compression configuration. It is generally referred to as the spectral gain curve of the microbunching instability. The first two subsections, III A and III B, describe our calculations on the spectral gain curve of SwissFEL, the mitigation of the microbunching instability with the laser heater and its impact on the final FEL intensity. The following subsection (III C) contains simulation results showing a deformation of the beam longitudinal phase space, which, as we mentioned before, is harmful for the preservation of the beam quality along the machine. In the last subsection (III D) we discuss the use of a long-response-time material for the photocathode as a possible way to mitigate the microbunching instability.

Table IV lists the relevant beam and machine parameters that we assume for our simulations.

A. Spectral gain of the microbunching instability

Studies on the microbunching instability usually introduce the initial bunching factor b_0:

$$b_0(k_0) = \frac{1}{Nec}\int I_0(z_0)e^{-ik_0z_0}dz_0, \qquad (1)$$

where $I_0(z_0)$ is the initial current profile as a function of the longitudinal coordinate along the bunch z_0, e the electron

TABLE IV. Beam and machine parameters of the first bunch compressor used in the simulations.

Parameters	
Beam energy at the laser heater (MeV)	130
Energy at the bunch compressor (MeV)	300
Normalized projected emittance (μm)	0.453
Relative uncorrelated energy spread at the LH	2.2×10^{-6}
Mean β-function along the laser heater (m)	35
Dipole length (m)	0.25
Dipole distance (m)	1.50
Dipole angle (deg)	3.82
Compression factor	6–12

charge, c the speed of light, k_0 the wave number of the current modulation, and N the number of electrons in the bunch. A similar expression defines the final bunching factor $b_F(k_F)$, where the current distribution is that at the location of evaluation (e.g., behind the first bunch compressor). Since the bunch is compressed the central wave number k_F of the modulation also changes with the compression factor C according to $k_F = Ck_0$. The microbunching instability gain at any given location along the machine is defined as:

$$G(k_0) = \left| \frac{b_F(Ck_0)}{b_0(k_0)} \right|. \quad (2)$$

The current profile at this location can then be predicted from the Fourier components of the initial bunch distribution and the spectral gain curve.

Several numerical codes are available to simulate collective effects in linac based machines. We use Astra [23], which includes both longitudinal and transverse space-charge-force calculations, to simulate the dynamics of the electron bunches along the low-energy section of the photoinjector from the emission at the cathode down to the exit of the second S-band cavity. At this location, where for our beam conditions the transverse space-charge forces are negligible, we switch to a faster code, ELEGANT [24], which does consider space charge and coherent synchrotron radiation (CSR), but exclusively along the longitudinal direction. To simulate the gain curve of the microbunching instability we modulate the distribution at the interface between ASTRA and ELEGANT, right before the laser heater location, with an additional current modulation featuring varying amplitude and periodicity. We then track the distribution and analyze its frequency content in the current profile at various locations.

In Fig. 3 we compare the outcome of our numerical simulations with the expectations of the analytical model described in [25]. Note that, for the sake of comparison, CSR effects are not included in the simulation shown, as they are not included in the analytical model either. Including CSR effects in the magnetic chicanes raises

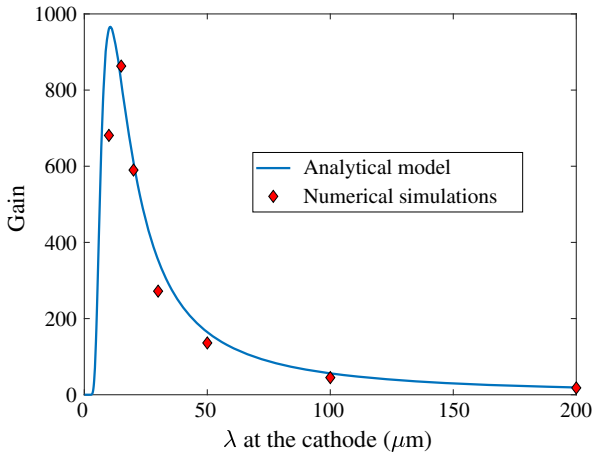

FIG. 3. Microbunching instability gain at the exit of the first bunch compressor as a function of modulation wavelength at the cathode from numerical simulation (excluding CSR effects) and from an analytical model [25].

the gain by about 10%, which shows that the amplitude gain is dominated by longitudinal space charge effects in the accelerating linac. More details can be found in [26]. To study the convergence in the determination of the gain factor we repeat the simulations for different numbers of particles (between 1 and 16 million) and different amplitudes of the imposed current modulation. Good convergence is obtained for 4 million particles and an amplitude of 0.5% [26].

B. Impact of laser heater

The laser heater [8,9] is an experimentally proven system for the efficient mitigation of the microbunching instability [27,28]. The uncorrelated energy spread induced by this device, $\Delta E/E_0$, is given by [25]:

$$\frac{\Delta E}{E_0} = \sqrt{\frac{P_L}{P_0}} \frac{KL_u}{\gamma_0 \sigma_r} \times \exp\left(-\frac{r^2}{4\sigma_r^2}\right) f\left[J_0\left(\frac{K^2}{4+2K^2}\right), J_1\left(\frac{K^2}{4+2K^2}\right)\right], \quad (3)$$

where P_L is the peak laser power, P_0 is a constant equal to 8.7 GW, $f[J_0(\frac{K^2}{4+2K^2}), J_1(\frac{K^2}{4+2K^2})]$ is a function of the Bessel functions J_0 and J_1, K is the undulator parameter, σ_r is the rms laser spot size along the undulator, r is the radius of the beam, and γ_0 is the Lorentz factor corresponding to E_0. The parameters and other details of the SwissFEL laser heater can be found in [14].

To determine the laser heater's impact on the spectral gain of the instability, we artificially increase in our simulations the slice energy spread by adding to the initial slice distribution a Gaussian distributed noise of different amplitudes $\Delta E/E_0$ at the location of the laser heater. In Fig. 4 we show the resulting dependence of the spectral

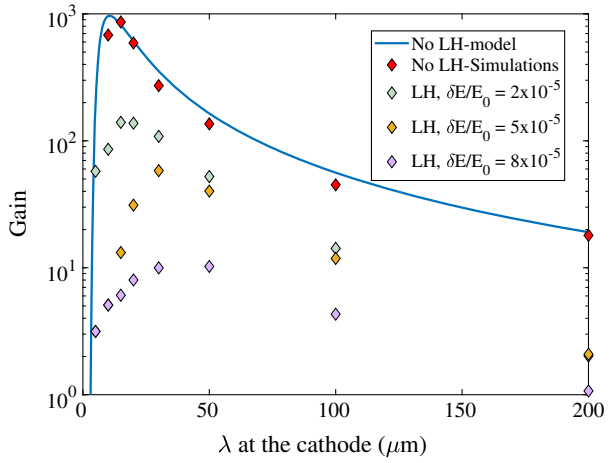

FIG. 4. Simulated spectral gain at the exit of the first bunch compressor assuming different values for the uncorrelated energy spread $\Delta E/E_0$ induced by the laser heater. The curve from the analytical model from Fig. 3 (no laser heater) is overlaid for comparison.

gain on $\Delta E/E_0$. Like in other facilities, the laser heater efficiently damps the instability in the region of maximum gain but it is less effective at longer wavelengths. Damping the modulations in this region would require stronger heating, at the expense of an increase of the energy spread, possibly beyond levels that are still acceptable for the FEL amplification process. Figure 5 illustrates the degradation of the saturation power, normalized to the case without laser heater, as a function of the induced relative uncorrelated energy spread. Here the saturation power was calculated based on Ming Xie's parametrization [29] applied to SwissFEL. The extent of heating $\Delta E/E_0$ therefore is a compromise between the full suppression

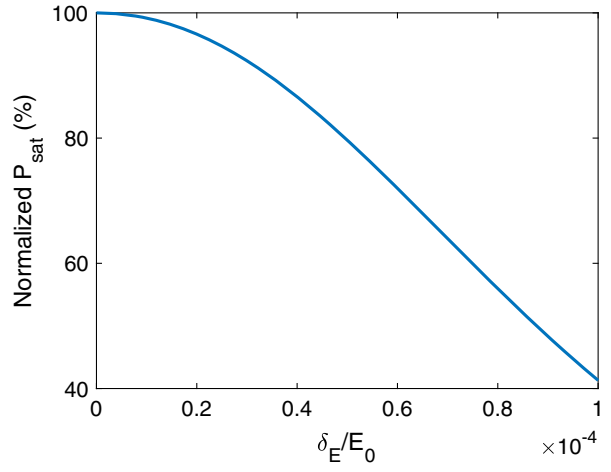

FIG. 5. Expected degradation of the FEL power (saturation power normalized to the case without laser heater) as a function of the relative uncorrelated energy spread induced by the laser heater, calculated for the SwissFEL Aramis line at 0.1 nm photon wavelength.

of the modulations susceptible to microbunching instability and a degradation of the lasing intensity due to the increase of energy spread.

In conclusion, within the range relevant for pulse stacking (e.g., the case of 16 subpulses listed in Table II, corresponding to about 200 μm, corresponding to 100 μm in presence of the beam longitudinal phase space fragmentation discussed in Sec. IV A), the microbunching instability gain is higher at smaller wavelengths (the maximum corresponds to few tens of μm) of the initial modulations. In this regime the laser heater represents an efficient method to damp the instability, albeit at the expense of an increased energy spread of the beam. By contrast, microbunching is subject to less gain at longer wavelengths, but is harder to suppress with a laser heater.

C. Longitudinal phase space fragmentation under compression

Under certain conditions of bunch charge, compression, beam energy, and drift lengths in the machine, space charge effects may be so strong as to modify the spectral content of the initial longitudinal structures from the pulse-stacked laser profile [30,31]. In such cases Eq. (2) is not valid anymore, as we are in the nonlinear regime of the instability. Clearly, if this effect shifts the frequency of the initial modulations toward the maximum of the spectral gain of the microbunching instability, then the final FEL performance will be degraded more than what is to be expected from the gain curve. We have dedicated some studies to this phenomenon, which we describe in the following.

In the low-energy section of a photoinjector, the electron bunch is subject to strong space-charge forces. The longitudinal component of these forces is proportional to the derivative of the longitudinal current profile of the bunch. In particular on the slopes of each of the Gaussian subpulses making up the approximate flat-top profile in the pulse-stacking scheme the particles at the head and the tail are pushed away from the center of the stack. As a consequence each single pulse evolves into a bifurcated distribution, thereby shifting the modulations of the electron bunch toward higher frequencies. The shorter the duration σ_t of each subpulse, the larger the force and consequently the deformation of the electron bunch profile.

As in the previous subsection, we study the dynamics of the beam using the ASTRA and ELEGANT codes in cascade. In the generation of the stacked laser profile we assume 8 subpulses and vary the duration of each subpulse between 100 fs and 600 fs. The simulation results, presented in Fig. 6, correspond to the case of the maximum compression factor achieved during the measurements discussed in Sec. IV. We see that subpulse durations on the order of 400 fs or larger result in a final distribution that is either smooth or carries a modulation with frequency equal to that of the laser distribution. For smaller subpulse durations we obtain a beam distribution with frequency components that

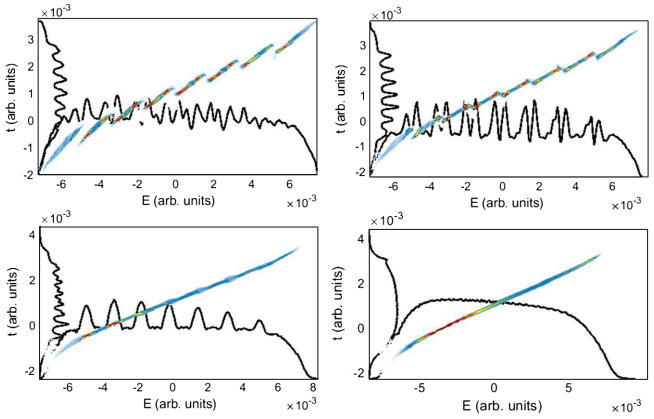

FIG. 6. Simulated longitudinal phase space (time t and energy E) of the electron beam after compression assuming for the generation at the photocathode a laser longitudinal profile consisting of 8 stacked subpulses. A compression factor of 12 is applied. From top left to bottom right the assumed subpulse durations are 100 fs, 300 fs, 400 fs, and 600 fs. The total charge is 200 pC and the total pulse duration is 10 ps (FWHM) for all cases.

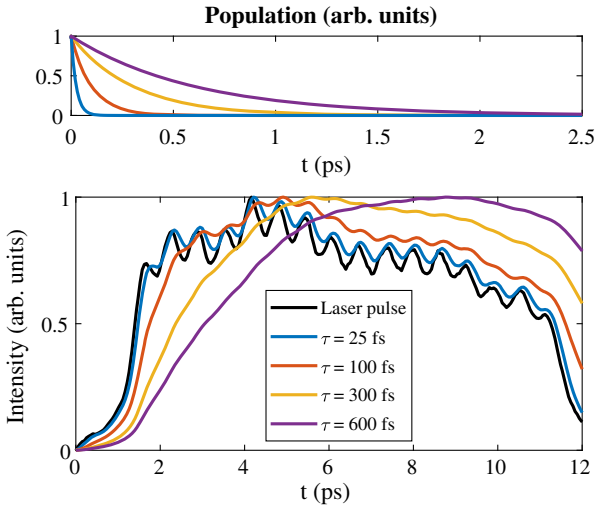

FIG. 7. Top: Response function assumed in the calculations for different photocathode material response times τ indicated in the legend. As a response function of the photocathode we assumed an exponential time decaying function with time constant equal to τ. Bottom: Expected electron bunch longitudinal proles at the photocathode assuming the measured laser prole consisting of 16 stacked subpulses, see Fig. 9.

are different with respect to the laser profile. In this regime each of the inner Gaussian pulses splits in two subpulses, resulting in the expected bifurcation pattern. For these inner Gaussians the expansion of each single pulse is counteracted by the neighboring stack, whereas for the pulses at the beginning and the end of the bunch the lack of this constraint leads to longer tails toward the charge-free region. Overall the number of final pulses is doubled with respect to the number of initial subpulses in the laser profile, and the spectral content of the modulations on the electron bunch is shifted to frequencies more harmful in view of microbunching instability. This issue must therefore be considered in the optimization of the stacking profile, as it prevents the use of short pulses to build up the flat-top distribution.

D. Damping of the current modulations using a long response time material

The microbunching instability may be initiated by shot-noise modulation of the electron bunch or by any initial modulation on the laser profile in a spectral region where the amplification process is efficient (or both). As mentioned above a possible way to reduce the current modulations and to mitigate the splitting of the single subpulses of the stacking is to use a photocathode which is made of a material characterized by a long response time with respect to the periodicity of the oscillations of the laser longitudinal profile. The longitudinal electron bunch is the convolution of the laser profile and the response time of the photocathode material.

The emission of electrons from a semiconductor photocathode, like Cs_2Te is a diffusionlike process with time constants on the order of 300 fs. In [11] a response time of 370 fs was reported. Earlier, in the absence of direct measurements for Cs_2Te, [32] quoted an effective response time on the order of 300 fs based on numerical simulations [33,34]. In Fig. 7 we show expected current profiles at the cathode illuminated with the measured laser pulse built from 16 Gaussian subpulses, convolved with an exponential decay function featuring different response times τ.

Obviously, the shorter the response time of the photocathode material, the closer the electron bunch profile resembles the laser profile. Conversely, for larger response times the structures on the laser profile are smoothed away and ultimately no longer present on the electron bunch. Thus by adopting a long-response-time material we expect less modulations in the beam current profile, thereby avoiding the spikes in the beam longitudinal phase space and hence the bifurcation of the subpulses. Accordingly, when using a laser heater—which, as shown above, efficiently suppresses the amplitude of the microbunching curve with the penalty of a reduction in lasing intensity due to the increased energy spread—the induced energy spread required to damp the instability is also expected to be smaller when operating with a long-response-time photocathode material.

IV. EXPERIMENTAL RESULTS

Our measurements were performed with two laser profiles. The first consists of 8 subpulses with individual durations of 300 ± 40 fs, obtained with 3 crystals (see Fig. 8). The second profile, obtained with 4 crystals, contains 16 subpulses with durations of 420 ± 40 fs

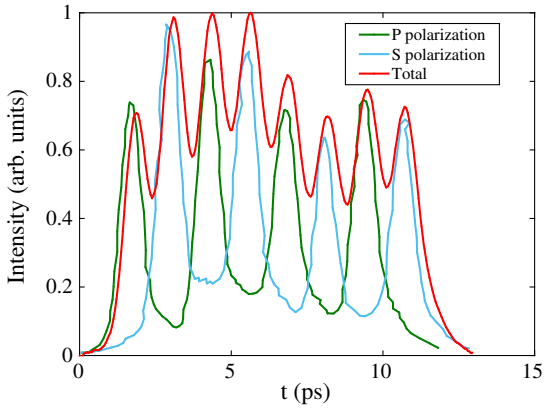

FIG. 8. Measured laser profile obtained using 8 stacked subpulses. The pulses of the two orthogonal polarizations are indicated as blue and green lines, the total pulse is represented by a red line. Each subpulse has a duration of 300 ± 40 fs and extracts about 25 pC of charge.

(see Fig. 9). The stacking parameters (charge and spacing of the subpulses) are adjusted to obtain a profile corresponding to the maximum charge SwissFEL design bunch. For the resulting pulse length and charge density we expect to observe the bifurcation in longitudinal phase space as discussed in Sec. III C. While the second configuration (with 16 subpulses) yields a smoother longitudinal profile, its frequency content is more harmful in terms of the microbunching instability, because it is closer to the maximum of the gain curve (compare Fig. 3 and Table II).

In Sec. IV A we present measurements in which we investigate the evolution of the bunch generated by the illumination of a copper cathode with different configurations of stacked profiles. We characterize the nonlinear effect on the beam longitudinal phase space as a function of the compression factor, similar to what has been presented

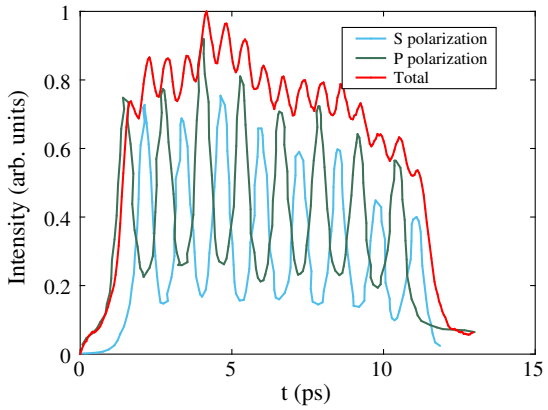

FIG. 9. Measured laser profile obtained using 16 stacked subpulses. The pulses of the two orthogonal polarizations are indicated as blue and green lines, the total pulse is represented by a red line. Each subpulse has a duration of 420 ± 40 fs and extracts about 12.5 pC of charge.

in Sec. III C with numerical simulations. In Sec. IV B, finally, we show experimentally how the use of a photocathode material with longer response time is an efficient method to counteract the amplification of the microbunching instability.

A. Longitudinal beam dynamics of a compressed bunch

To study nonlinear compression effects on an electron bunch generated from a pulse-stacked laser pulse we illuminated a copper cathode with the laser profiles shown in Figs. 9 and 8. We then varied the final bunch length by changing the off-crest phase of the cavities upstream of the magnetic chicane while keeping the longitudinal dispersion of the chicane constant. For the two compression settings corresponding to compression factors of 6 and 12 we measured the current profile and the longitudinal phase space in the diagnostics section downstream of the compressor. The results are shown in Figs. 10 and 11. The modulations along the longitudinal profile of the bunch are still visible in all cases, until we reach the resolution limit of the measurement. Also the longitudinal phase space of the beam clearly shows, at all compression settings, the structures imprinted by the modulations of the longitudinal laser profile. However, as predicted by simulation, the number of spikes is almost doubled with respect to the number of subpulses of the laser profile. This effect is more pronounced in the case with 8 subpulses, since there the diagnostics resolution is more adequate. For the stronger compression setting, the different behavior of the outer subpulses with respect to the inner ones is also observed, just as anticipated by our simulation results.

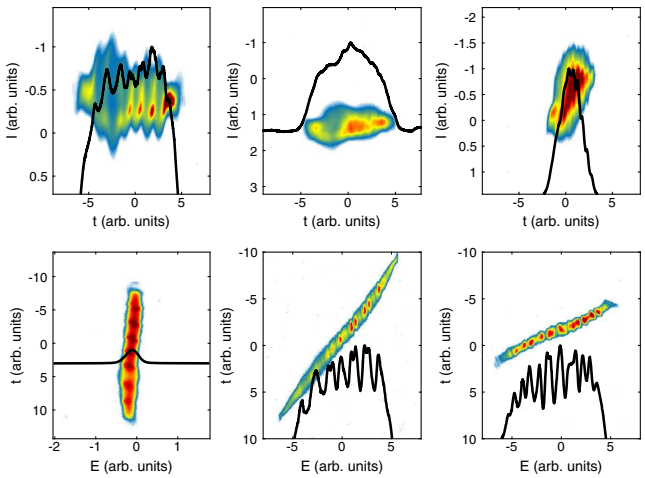

FIG. 10. Measured bunch current profiles (top row) and beam longitudinal phase space (bottom row) at the end of the injector corresponding to the laser profile shown in Fig. 8 without compression (left column), and for a compression factor of 6 (middle column), and 12 (right column). The copper cathode is used to generate the electron bunch.

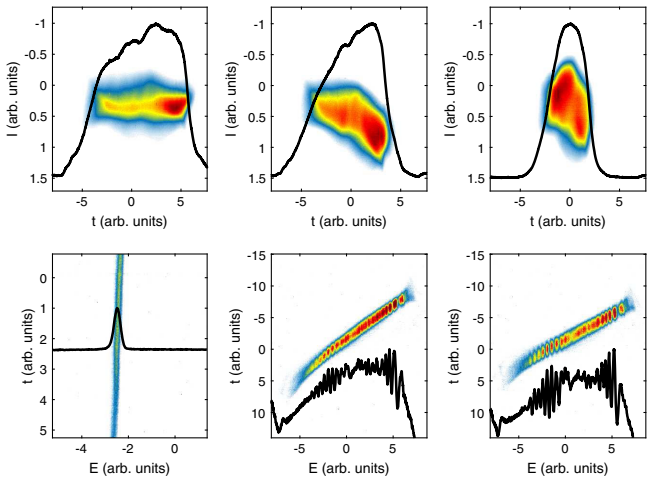

FIG. 11. Measured bunch current profiles (top row) and beam longitudinal phase space (bottom row) at the end of the injector corresponding to the laser profile shown in Fig. 9 without compression (left column), and for a compression factor of 6 (middle column), and 12 (right column). The copper cathode is used to generate the electron bunch.

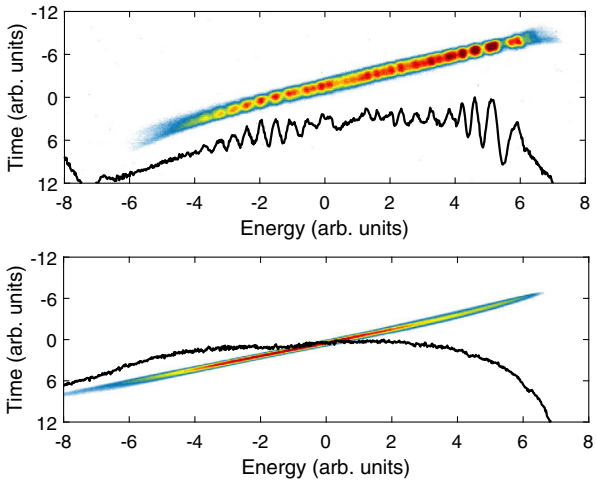

FIG. 12. Measured longitudinal phase space distribution of an electron bunch emitted from a copper (top) and a Cs_2Te photocathode (bottom) illuminated by the laser profile obtained by stacking 16 subpulses. In both cases the bunch compression factor is 6, at the beam energy of 200 MeV. The bunch charge is 200 pC in the case of the Cs_2Te cathode, but only 100 pC in the case of the copper cathode, which suffered from poor quantum efficiency. Therefore, space-charge effects are smaller in this case.

In summary we have shown, both in simulation (Sec. III C) and experimentally (this Section), that under certain conditions—subpulses with durations on the order of a few hundreds of fs, beam parameters similar to the SwissFEL case—the spikes in the bunch current profile imprinted by the stacked laser profile may split in two. This is in contrast to the basic theory of the microbunching instability, where the number of intensity modulations is constant along the machine. This bifurcation effect introduces dangerous high-frequency components in the response of the machine, where the gain is typically larger. We conclude that the stacking technique for the generation of an approximate flat-top laser profile in the photoinjector, when used in conjunction with a copper cathode, may be not ideal for driving an FEL.

B. Long- and short-response-time materials

In the last decades several photocathode materials have been investigated as alternatives to the commonly used copper, mainly to maximize the flux of electrons per photon illuminating the cathode (quantum efficiency) [35]. One of the most attractive materials for the application in photoinjectors is Cs_2Te, a semiconductor with high quantum efficiency (more than two orders of magnitude higher than copper), which reduces the requirements on the laser energy, and the relatively good intrinsic emittance, comparable to that of copper [36].

Cs_2Te has a significantly longer response time than copper. To study the effect of the longer response time on the compressed beam we illuminated a Cs_2Te cathode with the laser profile obtained with 16 subpulses shown in Fig. 9, and again compressed the beam in the magnetic chicane. After propagation to the end of the machine we measured the longitudinal phase space of the beam. The result, presented in Fig. 12 and compared to a measurement with a copper cathode, clearly shows how the structures due to the initial laser modulations are washed out in the case where a Cs_2Te photocathode is used to generate the electron bunch, as expected from our considerations in Sec. III D.

The measured profile shown in the bottom part of Fig. 12 should be compared to that shown in Fig. 7. The only mechanism enhancing the structures present at the time of emission is the microbunching gain during transport and compression. The comparison of the two profiles allows the qualitative conclusion that the response time of the Cs_2Te photocathode is of the order of 300 fs, consistent with the values quoted in [11,32].

We have thus demonstrated experimentally that the use of a long-response-time cathode material represents a viable approach to strongly reduce laser generated modulations on the bunch current profile, which may trigger or enhance the microbunching instability. While the focus of our studies lay on the longitudinal profile generated applying the stacking technique, this conclusion is valid in general for any laser longitudinal profile with oscillations of periodicity smaller than the response time of the photocathode material. The LH and the long-response-time photocathode material reduces the impact of the microbunching instability on the final FEL performances with different mechanisms. The first reduces the amplification gain more efficiently in the spectral region up to 150 μm, as shown in Fig. 4. The latter does not modify the gain curve,

but reduces one of the possible sources of the instability in a spectral range up to the response time of the photocathode material. As noted earlier, a cathode material with long response time will also reduce the energy spread required to be induced by a laser heater, thereby enhancing the ultimate FEL performance.

V. CONCLUSIONS

Electron beams with uniform mismatch and slice emittance along most of the bunch are an essential prerequisite for efficient lasing at an FEL. To achieve this goal with a photoinjector, the generation of an approximately flat-top longitudinal laser profile applying the pulse-stacking technique appears to be an attractive approach. A drawback of this method is given by the inevitable modulations of the charge along the pulse, determined by the number of subpulses, their duration and spacing.

When a copper cathode is used, a frequent choice in photoinjectors, the short response time of this material implies that the electron beam profile will be a replica of the laser profile, including its modulations due to the subpulses. We have seen that already a modest compression of the beam enhances these structures. Further we have shown, both in simulation and in experiment, that at stronger compression, each of the subpulses splits in two, generating a double-horn structure in the longitudinal phase space of the beam. This effect may be very harmful because it shifts the frequency content of the electron beam toward frequencies where the microbunching amplification gain is larger or even at its maximum.

Our observations imply that the use of a copper photocathode in conjunction with the pulse-stacking technique for the generation of the laser profile is not well suited for driving a photoinjector-based FEL with several compression stages. A possible way out consists in exploiting a photocathode characterized by a longer response time, such as Cs_2Te. We have demonstrated experimentally that in this case the longitudinal phase space of the electron beam after compression is much smoother than in the case of a copper cathode. The use of photocathode materials with long response time therefore represents a viable approach to mitigate the microbunching instability or simply diminish the energy spread required to be induced from a laser heater.

Both the application of a laser heater and the utilization of a photocathode characterized by a long response time are viable approaches to mitigate the microbunching instability. The laser heater reduces the amplification of initial density modulations in the region of a few tens of μm, where the gain is maximal for FEL facilities. By contrast a long-response-time cathode does not modify the gain curve, but suppresses the initial fluctuations in the spectral region below the response time. In the case of Cs_2Te with a response time on the order of a few hundred fs this corresponds to the region up to a few hundred μm. Both methods may be applied at the same time and complement each other to achieve optimal FEL performance.

ACKNOWLEDGMENTS

We are indebted to all PSI expert groups and the SwissFEL team for their efforts in the construction and operation of the SwissFEL Injector Test Facility, P. Craievich for his precious comments, and H. H. Braun for the fruitful discussions and the proofreading of the manuscript.

[1] J. S. Fraser, R. L. Sheffield, E. R. Gray, and G. W. Rodenz, High-brightness photoemitter injector for electron accelerators, IEEE Trans. Nucl. Sci. **32**, 1791 (1985).

[2] M. Huening, P. Piot, and H. Schlarb, Observation of longitudinal phase space fragmentation at the TESLA test facility free-electron laser, Nucl. Instrum. Methods Phys. Res., Sect. A **475**, 348 (2001).

[3] D. Huang, C. Feng, H. Deng, Q. Gu, and Z. Zhao, Transverse to longitudinal phase space coupling in an electron beam for suppression of microbunching instability, Phys. Rev. Accel. Beams **19**, 100701 (2016).

[4] R. Ischebeck, E. Prat, V. Thominet, and C. O. Loch, Transverse profile imager for ultrabright electron beams, Phys. Rev. Accel. Beams **18**, 082802 (2015).

[5] S. Di Mitri and S. Spampinati, Microbunching Instability Suppression via Electron-Magnetic-Phase Mixing, Phys. Rev. Lett. **112**, 134802 (2014).

[6] E. Prat, E. Ferrari, S. Reiche, and T. Schietinger, Using the optical-klystron effect to increase and measure the intrinsic beam energy spread in free-electron-laser facilities, Phys. Rev. Accel. Beams **20**, 040702 (2017).

[7] C. Behrens, Z. Huang, and D. Xiang, Reversible electron beam heating for suppression of microbunching instabilities at free-electron lasers, Phys. Rev. Accel. Beams **15**, 022802 (2012).

[8] Z. Huang *et al.*, Measurements of the LCLS laser heater and its impact on the x-ray FEL performance, Report No. SLAC-PUB 13854, 2009.

[9] E. L. Saldin, E. A. Schneidmiller, and M. V. Yurkov, Longitudinal space charge-driven microbunching instability in the TESLA Test Facility linac, Nucl. Instrum. Methods Phys. Res., Sect. A **528**, 355 (2004).

[10] W. E. Spicer and A. Herrera-Gomez, Modern theory and applications of photocathodes, Report No. SLAC-PUB-6306, 1993.

[11] A. Aryshev, M. Shevelev, Y. Honda, N. Terunuma, and J. Urakawa, Femtosecond response time measurements of a Cs_2Te photocathode, Appl. Phys. Lett. **111**, 033508 (2017).

[12] R. Ganter *et al.*, SwissFEL Conceptual design report, Technical Report Paul Scherrer Institute, 2011.

[13] C. Milne *et al.*, SwissFEL: The Swiss X-ray Free Electron Laser, Appl. Sci. 2017 **7**, 720 (2017).

[14] M. Pedrozzi, M. Calvi, R. Ischebeck, S. Reiche, C. Vicario, B. D. Fell, and N. Thompson, The laser heater system of SwissFEL, in *Proceedings of the Free Electron Laser*

Conference 2014, Basel (Switzerland) (JACoW, CERN, Geneva, 2014), p. 871.

[15] T. Schietinger *et al.*, Commissioning experience and beam physics measurements at the SwissFEL Injector Test Facility, Phys. Rev. Accel. Beams **19**, 100702 (2016).

[16] A. Trisorio, M. Divall, C. Vicario, C. P. Hauri, and A. Courjaud, New concept for the SwissFEL gun laser, in *Proceedings of the Free Electron Laser Conference 2013, New York, (NY, USA)* (JACoW, CERN, Geneva, 2013), p. 442.

[17] I. V. Bazarov, D. G. Ouzounov, B. M. Dunham, S. A. Belomestnykh, Y. Li, X. Liu, R. E. Meller, J. Sikora, and C. K. Sinclair, Efficient temporal shaping of electron distributions for high-brightness photoemission electron guns, Phys. Rev. Accel. Beams **11**, 040702 (2008).

[18] A. Trisorio, P. M. Paul, F. Ple, C. Ruchert, C. Vicario, and C. P. Hauri, Ultrabroadband TW-class Ti:sapphire laser system with adjustable central wavelength, bandwidth and multi-color operation, Opt. Express **19**, 20128 (2011).

[19] R. Ganter *et al.*, SwissFEL cathode load-lock system, in *Proceedings of the Free Electron Laser Conference 2013, New York, (NY, USA)* (JACoW, CERN, Geneva, 2013), p. 259.

[20] J. Bossert *et al.*, Cu and Cs_2Te cathodes preparation and QE history at the SwissFEL Injector Test Facility, in *Proceedings of the Free Electron Laser Conference 2014, Basel (Switzerland)* (JACoW, CERN, Geneva, 2014), p. 832.

[21] J. Wu, P. Emma, Z. Huang, and C. Limborg, Temporal profile of the LCLS photocathode ultraviolet drive laser tolerated by the microbunching instability, Reports No. SLAC-PUB-10430 and No. LCLS-TN-04-6, 2004.

[22] M. Borland, Modeling of the microbunching instability, Phys. Rev. Accel. Beams **11**, 030701 (2008).

[23] K. Floettmann, http://www.desy.de/~mpyflo/Astra_dokumentation/ (2000).

[24] M. Borland, elegant: A flexible SDDS-compliant code for accelerator simulation, Advanced Photon Source Report No. LS-287, 2000.

[25] Z. Huang, M. Borland, P. Emma, J. Wu, C. Limborg, G. Stupakov, and J. Welch, Suppression of microbunching instability in the linac coherent light source, Phys. Rev. Accel. Beams **7**, 074401 (2004).

[26] S. Bettoni, B. Beutner, and V. A. Goryashko, Microbunching instability studies in SwissFEL, in *Proceedings of the Particle Accelerator Conference 2012, New Orleans (FL, USA)* (JACoW, CERN, Geneva, 2012), p. 1744.

[27] S. Spampinati *et al.*, Laser heater commissioning at an externally seeded free-electron laser, Phys. Rev. Accel. Beams **17**, 120705 (2014).

[28] J. Lee, J.-H. Han, S. Lee, J. Hong, C. H. Kim, C. K. Min, and I. S. Ko, PAL-XFEL laser heater commissioning, Nucl. Instrum. Methods Phys. Res., Sect. A **843**, 39 (2017).

[29] M. Xie, Design optimization for an X-ray free electron laser driven by SLAC linac, in *Proceedings of the 16th Particle Accelerator Conference, Dallas (TX, USA) 1995* (IEEE, Piscataway, NJ, 1996), p. 183.

[30] D. Filippetto, P. Musumeci, M. Zolotorev, and G. Stupakov, Maximum current density and beam brightness achievable by laser-driven electron sources, Phys. Rev. Accel. Beams **17**, 024201 (2014).

[31] D. H. Dowell, S. Joly, A. Loulergue, J. P. de Brion, and G. Haouat, Observation of space-charge driven beam instabilities in a radio frequency photoinjector, Phys. Plasmas **4**, 3369 (1997).

[32] P. Piot, Y.-E Sun, T. J. Maxwell, J. Ruan, E. Secchi, and J. C. T. Thangaraj, Formation and acceleration of uniformly filled ellipsoidal electron bunches obtained via space-charge-driven expansion from a cesium-telluride photocathode, Phys. Rev. Accel. Beams **16**, 010102 (2013).

[33] G. Ferrini, P. Michelato, and F. Parmigiani, A Monte Carlo simulation of low energy photoelectron scattering in Cs_2Te, Solid State Commun. **106**, 21 (1998).

[34] W. E. Spicer, Photoemissive, photoconductive, and optical absorption studies of alkali-antimony compounds, Phys. Rev. **112**, 114 (1958).

[35] D. H. Dowell, I. Bazarov, B. Dunham, K. Harkay, C. Hernandez-Garcia, R. Legg, and W. Wan, Cathode R&D for future light sources, Nucl. Instrum. Methods Phys. Res., Sect. A **622**, 685 (2010).

[36] E. Prat, S. Bettoni, H. H. Braun, R. Ganter, and T. Schietinger, Measurements of copper and cesium telluride cathodes in a radio-frequency photoinjector, Phys. Rev. Accel. Beams **18**, 043401 (2015).